PUBLICAÇÕES

UNIVERSIDADE DE SÃO PAULO

INSTITUTO DE FÍSICA
CAIXA POSTAL 20516
01498-970 SÃO PAULO - SP
BRASIL

IFUSP/P-1078

ANALYSIS OF NONLINEAR OSCILLATIONS BY GABOR SPECTROGRAMS

H. Franco
Instituto de Física, Universidade de São Paulo

R.M.O. Pauletti
Escola Politécnica, Universidade de São Paulo
São Paulo, SP, Brazil

Outubro/1993

ANALYSIS OF NONLINEAR OSCILLATIONS BY GABOR SPECTROGRAMS

H. Franco
Instituto de Física, Universidade de São Paulo, Caixa Postal 20516, 01498-970 São Paulo, SP, Brazil

and

R.M.O. Pauletti
Escola Politécnica, Universidade de São Paulo, São Paulo, SP, Brazil

Abstract. We examine the potentiality of the Gabor spectrogram as a tool for the study of the temporal behavior of nonlinear oscillators. Numerical simulations on a snap-through system and homogeneous Duffing equation are analyzed by this method. Gabor spectrograms show dynamic properties of nonlinear oscillators in situations where the conventional Fourier analysis are not appropriate.

Key words: Gabor transform, spectrogram, wavelet, snap-through, Duffing equation, digital signal processing

1 Introduction

Non-linearity limits the usefulness of some basic tools of linear dynamic analysis, such as the Fourier Transform (FT). The latter looses its power as concise description of the movement if the system is nonlinear. On the other hand, as we introduce new methods, it is desirable to preserve as far as possible our familiar tools and mathematical objects arisen from linear systems, while entering the domain of non linearity.

The Gabor Transform (Gabor, 1946), (Bastiaans, 1980), (Perelomov, 1971), (Bargmann*et al.*, 1971), (Quian, 1992A) and (Quian, 1992B) keeps many essential features of the FT, while adding time resolution. The power spectrum becomes then a function of both frequency *and* time. Many of the features of the FT are still distinguishable on each "time slice" of the Gabor Transform. In particular, if the motion becomes locally periodic, its harmonic series can be recognized as a family of equally spaced, albeit transient, "spectral lines". These properties make the Gabor transform a useful tool in the analysis of nonstationary phenomena ranging from eletroencephalography (Banquet, 1973) to plasma physics (Franco *et al.*, 1992).

In this work, we use the Gabor transform to analyse the free oscillations of a nonlinear *snap-through* oscillator. We perform numerical solutions of the differential equations with both the exact force law and with a cubic approximation, which is equivalent to a homogeneous Duffing equation. The Gabor spectrogram then allows us to discriminate the transformations of the spectral content of the motion, along the simulation time.

2 Gabor Spectrograms

The Fourier transform is an expansion of a function over a base of oscillating functions with the form of a complex argument exponential. The expansion coefficients are calculated by the scalar product of the function by each of the base elements in the Hilbert space (Courant and Hilbert, 1953). In the case of a discrete variable, such as in a numerical simulation, the FT is replaced by the discrete Fourier transform (DFT). For a discrete time function $s(t)$, the DFT reads:

$$S(f_j) = \sum_{T+1}^{N} s(t)\, g_j^*(t) \quad ; \qquad g_j = \exp(2\pi\, i\, f_j\, t) \quad , \tag{1}$$

where t is a time counting variable, the g_j are the base functions and the asterisk denotes complex conjugate (Oppenheim, 1989).

The FT is an economic description of the motion of linear systems, since most $S(f_j)$ vanish. With a single degree of freedom, we have a single lorentzian "spectral line", perhaps broadened to some extent by a damping effect. A sole coefficient accounts for a large number of points of a sinusoidal function in time domain. In the case of many degrees of freedom, we have as many eigenmodes, each corresponding to a single independent oscillator in a convenient coordinates system. This makes the set of base elements of the FT quite appropriate to describe linear dynamic systems. However, if the spectrum changes in time, the FT, while still a complete expansion of the function, is no longer a concise one. It does not account for the time evolution.

The lack of time resolution of the FT arises from the fact that the base elements give equal weights to all the points of the function, so that every time information is mingled. The Gabor transform brings time resolution to the base elements by multiplying each oscillating term by a set of Gaussian *window functions* with the median centered at different times t_k and a mean square deviation σ_t. The window function acts as a mask, selecting only a narrow slice of the time domain and screening the outside points. A single wave packet can then "tune in" a single narrow frequency band and a single time slice. A complete set of Gabor wave packets spans the two dimensional time-frequency domain. The discrete Gabor Transform reads then:

$$S\,(f_j, t_k) = \sum_{t=1}^{N} s(t)\, g_{jk}^*(t) \quad , \tag{2}$$

where the analysing base functions (wave packets) are defined as:

$$g_{jk} = \exp - \left(\frac{t - t_k}{2\sigma_t}\right)^2 \exp\left[2\pi\, i\, f_j\, (t - t_k)\right] \quad , \tag{3}$$

and $t_k = k\sqrt{2\pi}\,\sigma_t$.

The Fourier transform of the wave packet has in the frequency domain also a form of a Gaussian wave packet (Gabor, 1946). The frequency domain Gaussian

peak is, of course, centred at the wave packets own frequency, while the oscillating term is linked with the function displacement in time. However, the frequency and time mean square deviations σ_f and σ_t are linked through a constraint arisen from the wave packet definition: they have a constant product: $\sigma_f\,\sigma_t = 1/4\pi$. It can be shown that *any* other possible forms of the wave packets would have a greater product of time and frequencies mean square deviation or *uncertainties*. In general $\sigma_f\,\sigma_t \geq 1/4\pi$ ((Schiff, 1955), p. 67).

This is a general mathematical property of wave packets. It was borrowed from an equivalent problem of great conceptual importance on quantum mechanics, the *uncertainty principle*. The choice of Gaussian minimises then simultaneously the uncertainty of the base wave packets in time and frequency domains. This optimises the analysis resolution on the two-dimension time-frequency domain and brings symmetry between both variables since they have the same form on time and frequency domains.

The times and frequencies of the *Gabor grid* are:

$$t_k = k\sqrt{2\pi}\,\sigma_t \quad ; \qquad f_j = j\sqrt{2\pi}\,\sigma_f \quad , \tag{4}$$

The time domain is completely spanned by a grid of analyzing wave packets with frequencies and times $f_j\,t_k$. The number of possible values of t_k is N_s/t_k different time slices, where N_s is the number of discrete points of the function or simulation to be analysed. The highest frequency value attained by f_j is half the "sampling frequency" or half the number of simulation points per time unit. The total number of analyzing wave packets, which can be calculated from the above considerations and equations (4) is asymptotically equal to N_s, the number of points of the original function. The Gabor grid has thus as many independent numbers as the analysed function.

In figure 1 we show the form of this grid (a) and the form of the real part of a few wave packets (b) from a complete set, as well as their envelopes. Since the time-widths of all envelopes are equal, a variable number of cycles are enclosed inside the envelope for different frequencies f_j.

It is possible to perform the Gabor analysis in a grid of times and frequencies denser than one described above. In this case, we have the number of independent numbers of the expansion *larger* than that of the original function, and the expansion is *overcomplete* or *oversampled*. Some degree of oversampling may be desirable to enable an easier visual examination since the spectrogram becomes smoother. Although the just complete Gabor spectrogram contains all the information about the original function, it can result on a hardly readable graphic representation, with a mosaic of a few squares with discontinuous borders. Oversampling, while bringing an extra computational overhead, yields a more readable graphic display.

A number of different names were used for the Gabor discrete transform. When continuous variables are used for time and frequency, the method is called *Gabor transform*. Otherwise, the names discrete Gabor transform or Gabor matrix are employed. On the other hand, the word *spectrogram* was coined in the context of an

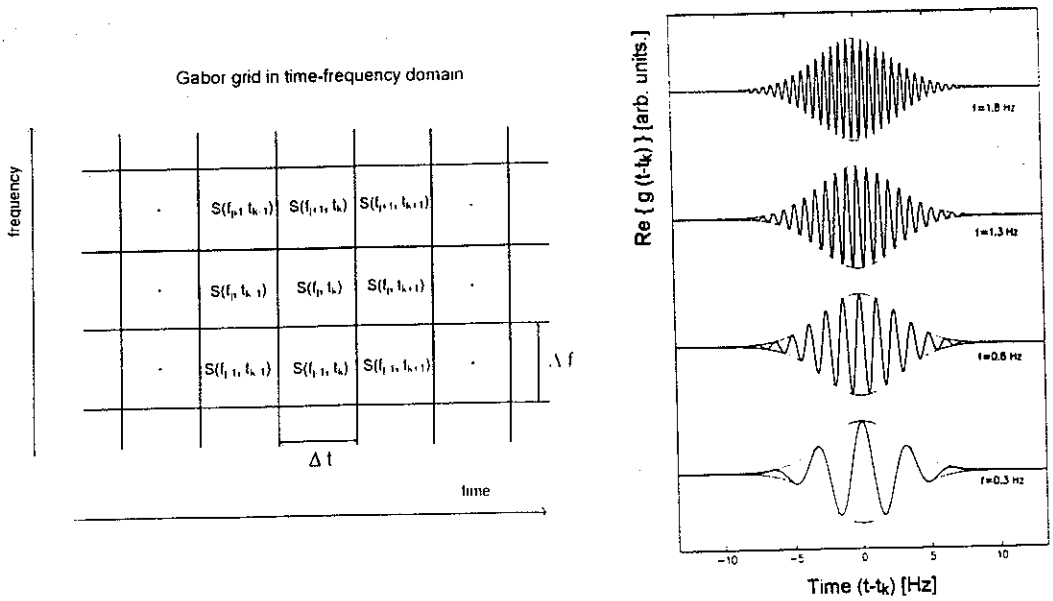

Fig. 1. Construction of the Gabor spectrogram: a) Gabor grid in the time-frequency domain; b) Examples of analyzing wave packets in the Gabor grid

analogue device invented in the 40' that performs a signal analysis very similar to the Gabor method, while using a different kind of envelope function. In this work, we shall refer to the latter as *Gabor spectrogram* (GS), whether it is oversampled or not. This name links the Gabor discrete transform with an electronic technique in use for decades in the analysis of human voice and animal sounds.

2.1 Why Not Wavelets?

We should also mention here the *wavelet transform*, quite related to Gabor spectrograms, that received great attention in the last years (Morlet *et al.*, 1982A) and ((Morlet *et al.*, 1982B); (Grossman, 1984); (Combes al., 1987), (Meyer, 1989), (Daubechies, 1990), (Daubechies *et al.*, 1992) & subsequent papers). It analyzes the function along different *scales*, rather than frequencies, and provides a better convergence during the function reconstruction. It is also a more acute analytical tool than Gabor Transform and possibly better suited to analyse a hard non-linear transient, where relevant phenomena are distributed through a wide range of time scales.

On the other hand, the wavelet transform involves a hardly intuitive variation of time resolution through the frequency range that makes delicate its interpretation.

The frequency scale is logarithmic, so that harmonic series are no longer recognizable by the signature of evenly spaced lines . Since the Gabor transform is also a good approximation of discrete wavelet transform on a narrow band of frequencies, we considered it a good compromise between efficiency and readability of results. Moreover, the phenomena here analyzed span less than a decade.

2.2 Elementary Examples

In order to provide some graphical insight about the method, we shall examine first an elementary case of the Gabor spectrogram. We show in figure 2a the time history of the displacement of a damped linear oscillator with a natural frequency 1 Hz, and in figure 2b, the corresponding (discrete) Fourier transform. Both frequencial and temporal behaviors of the system are displayed in the GS of figure 2c.

The spectrum exhibits a "keel" or "crest" located along the natural frequency of the system, 1 Hz. A higher oscillating frequency would displace the crest to the bottom. On the other hand, the crest profile mirrors the oscillation amplitude, showing the expected exponential decay envelope. Of course, in this simple linear case, the GS does not bring new insight. It may just serve as a guideline to understand more complex nonlinear cases.

Another simple example is a frequency modulated (FM) function (figure 3a). The frequency slowly migrates from 0.6 to 1.4 Hz. The DFT amplitude (figure 3b) shows a broadened peak with a flat irregular top that encloses the band of frequencies crossed by the function. It bears no information about the time changes. The GS (figure 3c) shows an inclined ridge that maps the function path on the time-frequency domain, masked on the Fourier transform.

3 The *Snap-through* (ST) System

3.1 System Description

The *snap-through* system (ST system) shown in figure 4a is one of the simplest geometrically non-linear truss structures. It represents however the essential features of a larger class of structures, like shallow frames, arches or shells (Holmes, 1979), (Karaesmen, 1992) which may present limit point instabilities (Thompson, 1973), (Thompson, 1984), (Huseyin, 1975), (Simetsen, 1990). The name "snap-through" derives from this property: under a sufficiently high compressive load, the original configuration looses its bearing capacity and the truss suddenly collapses, undergoing large displacements until a new stable configuration is reached.

Generally speaking, bifurcation instabilities are also possible for this system, depending on its parameters: lateral buckling of one or both rods or lateral buckling of the whole structure. Nevertheless, if we disregard the bending flexibility of the rods and assume symmetry about the vertical axis to hold, the system behavior may be described by only one degree of freedom. The vertical displacement x of the apex is a natural choice. In this case, the system parameters are those

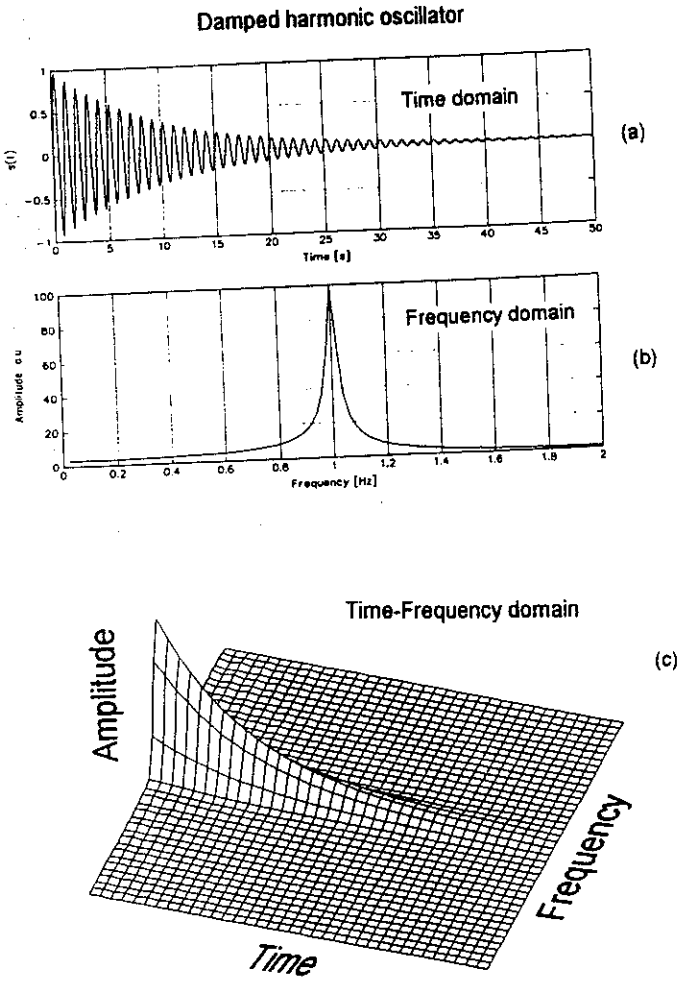

Fig. 2. Analysis of a damped linear oscillator: a) Time history; b) Fourier transform; c) Gabor spectrogram

depicted in figure 4b.

For the sake of simplicity, we assume here that the system remains linear elastic, regardless of the magnitude of the deformations it undergoes. We are concerned with spanning either large and small amplitude oscillations, but avoid inclusion of any material non linearity, thus avoiding changes in the characteristics of the equilibrium equation. This would introduce complications that could screen the

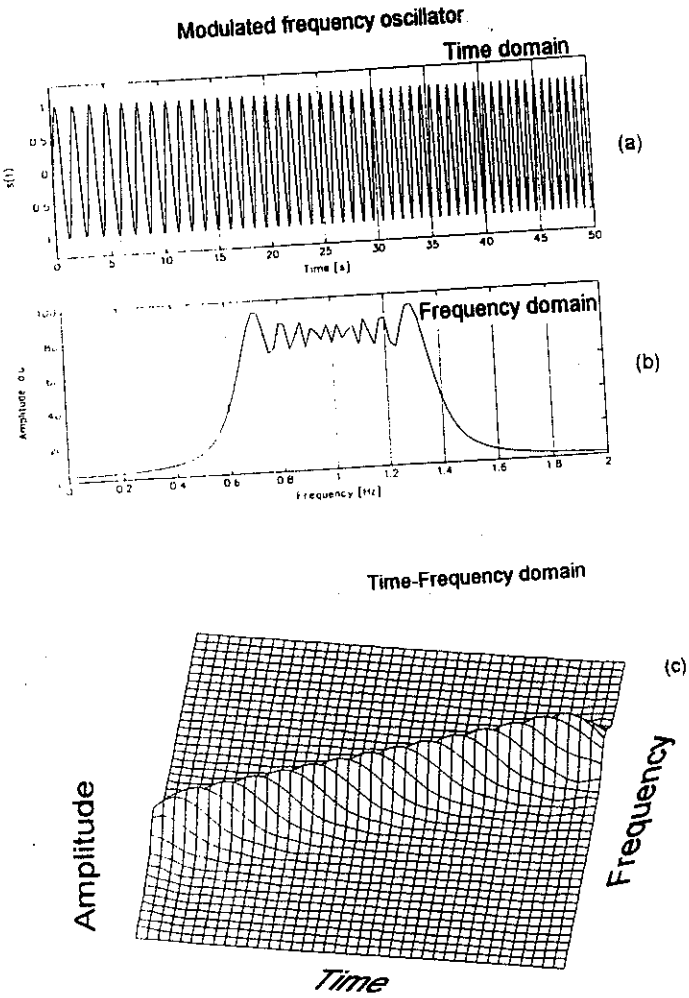

Fig. 3. Analysis of a frequency modulated oscillating function a) Time history; b) Fourier transform; c) Gabor spectrogram

basic properties of the S-T system.

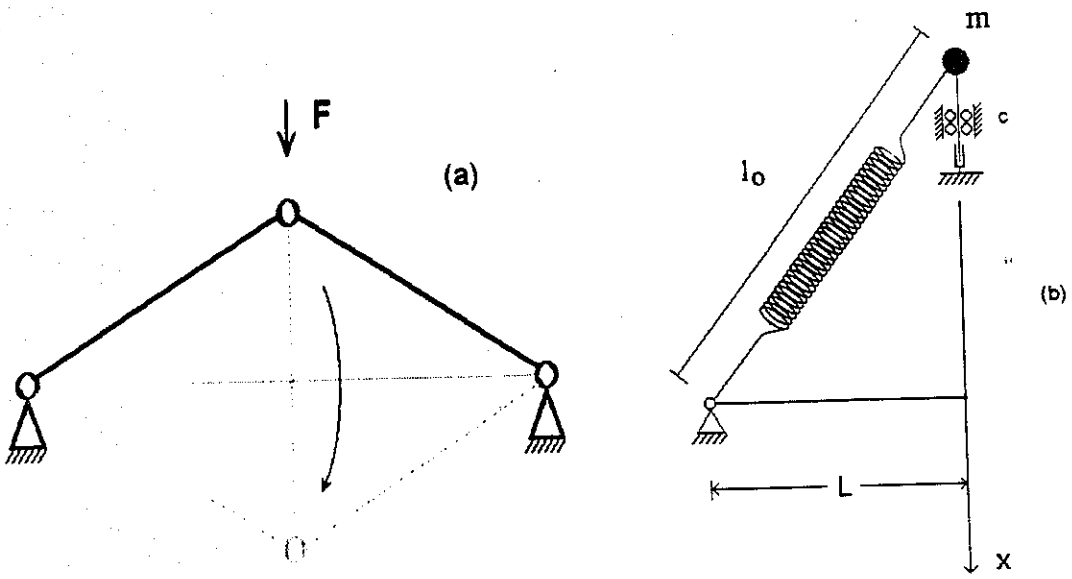

Fig. 4. Mechanical model of the "snap through" system, showing the names of variables: a) Structure depicting a snap-through system; b) A simplified model with a single degree of freedom

3.2 Equilibrium Equations

We deduce the dynamic equilibrium equation of the ST system from the Euler-Lagrange Equation (ELE):

$$\frac{d}{dt}\left(\frac{\partial \mathcal{L}}{\partial \dot{x}}\right) - \frac{\partial \mathcal{L}}{\partial x} = N \quad . \tag{5}$$

The Lagrangean function $\mathcal{L}$ is defined, for elastic systems and in absence of a potential field, as $\mathcal{L} = T - U$, where T is the kinetic energy and U is the energy of elastic deformation. The term N, in the right hand of the equation 5 includes all non-conservative forces acting upon the system.

For the ST system we thus have

$$T = \frac{1}{2} m \dot{x}^2 \tag{6}$$

$$U = \frac{1}{2} k(\ell - \ell_0)^2 \tag{7}$$

where m is the generalized mass of the system, $\dot{x}$ is the velocity of the apex, ℓ_0 is the undeformed length of the rod, $\ell = \sqrt{(x^2 + L^2)}$ its current length and $k = EA/\ell_0$ its spring constant. Now considering viscous damping and an oscillating external

force $F_0 \cos(\Omega t)$ acting upon the apex of the truss, and substituting in the ELE, we obtain the dynamic equilibrium equation of the ST system:

$$m\ddot{x} + c\dot{x} + k\left(1 - \frac{\ell_0}{\sqrt{x^2 + L^2}}\right) x = F_0 \cos(\Omega t) \tag{8}$$

where it can be seen that the system non-linearity arises from the restoring elastic force term

$$P(x) = k\left(1 - \frac{\ell_0}{\sqrt{x^2 + L^2}}\right) x \tag{9}$$

if we expand $P(x)$ in Taylor series we obtain

$$P(x) = k\left[1 - \frac{\ell_0}{L}x + \left(\frac{k}{2}\frac{\ell_0}{L^3}\right) x^3 + O(x^5)\right] \quad . \tag{10}$$

With this approximation, equation 8 is known as the Forced Duffing equation, well studied in the domain of nonlinear oscillations and chaos (Stoker, 1950), (Holmes, 1979), (Nayfeh, 1979), (Thompson, 1987). We may expect that the same sort of phenomena displayed by the Duffing equation exists also for the ST system. Nevertheless, we shall consider in this work exclusively the behavior of the system in damped free vibrations, with $p(t) = 0$. No chaotic behavior is possible is this case.

Moreover, if we consider the tangent stiffness of the system we have

$$k_T = \frac{dP(x)}{dx} = k\left\{1 - \frac{\ell_0}{\ell}\left[1 - \left(\frac{x}{\ell}\right)^2\right]\right\} \quad . \tag{11}$$

Now, clearly

$$\lim_{x \to \pm\infty} k_T = k \quad , \tag{12}$$

that is, for large displacements, the ST system tends to linear behavior. Instead, a 3rd order polynomial restoring force is non-linear regardless the intensity of the displacements. We used $k = 4\pi^2$; $L = 1.0$; $\ell_0 = \sqrt{2}$ and $m = 1$ so that the equilibrium points are $x = \pm 1$ and the system high amplitude frequency is 1 Hz. A linear damping $-c\dot{x}$ is also included on the model.

Figure 5a sketches the restoring elastic force $P(x)$ (both exact and the polynomial approximation), the elastic potential $U(x)$ (figure 5b) and the tangent stiffness k_T (figure 5c) as a function of the displacement of the system. The dashed area in figure 5b corresponds to the region of negative stiffness. In Figure 5d we show also the undamped phase trajectories for the ST system with different energy contents. The attraction basin clearly has two competing point attractors.

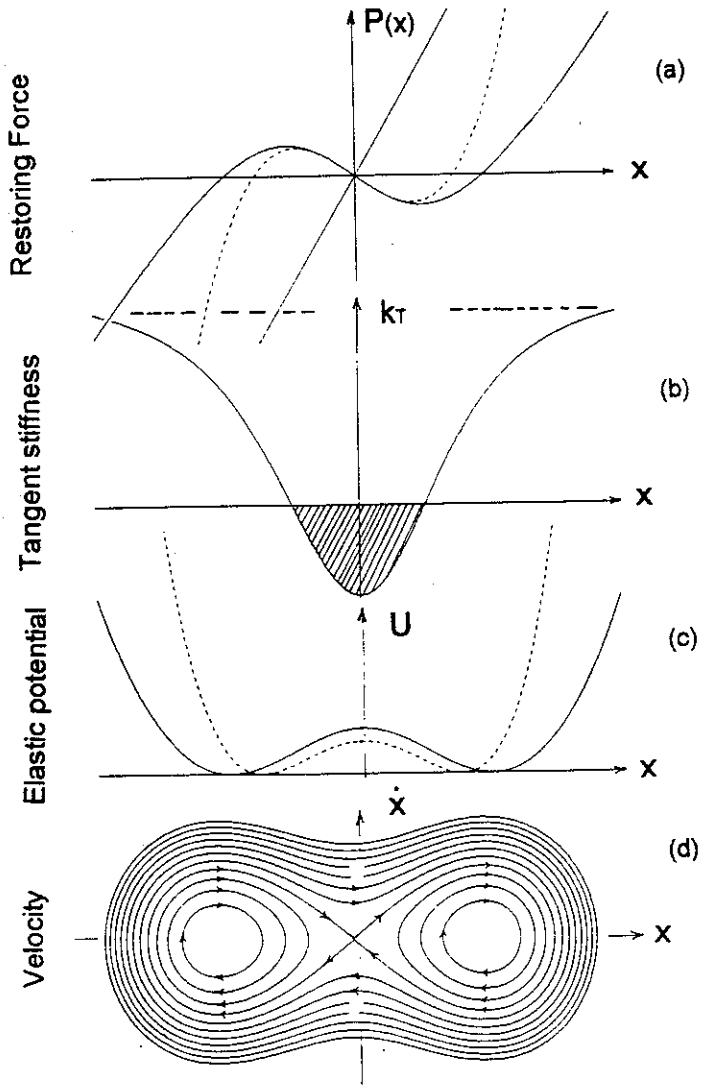

Fig. 5. Mechanical behavior of the snap-through system a) Restoring force; solid line: snap-through system; dashed line: polynomial approximation (homogeneous Duffing equation). The diagonal straight line corresponds to an equivalent linear oscillator; b) Elastic potential solid line: snap-through system; dashed line: polynomial approximation; c) Tangent stiffness; d) Phase space diagram of the snap-through system

4 Numerical Solutions

4.1 Calculation Algorithm

In our first simulations, we used the Newmark method, with a constant mean acceleration scheme (Bathe, 1976). However, this procedure proved to be satisfactory only in cases where considerable damping was present. For low damping, very small time-steps were required to avoid divergence of the solution (with the system energy being amplified up to an asymptotic limit); for zero damping, the divergence was unlimited.

These difficulties lead us to choose other algorithms to solve equation 8. The principal methods available to solve ordinary differential equations may be divided in single or multiple step methods, like the Runge-Kutta and the Adams methods respectively. Both types apply to a set of n first order differential equations, thus requiring dismembering equation 8 in a set of 2 equations. Detailed descriptions of these methods may be found in Curtis (1989) and Kahaner (1989). It can be shown that, whilst of different implementation, both types of method are essentially equivalent. When a regular spacing of the time steps is not required, the single step algorithms may be more economical (Kahaner al., 1989).

For the aims of the present work, however, we require the solution to be sampled at regular time intervals, in order to afterwards perform the calculation of its GS. In this case, multiple step methods may be more attractive. To perform the calculations presented in this work we chose the *Adams-Moulton* method, a predictor-corrector multi-step algorithm that displays twice the computational efficiency of the R-K method for the same degree of accuracy (Curtis, 1989). We have employed the DGEAR routine (IMSL Library 1984), which implements the A-M algorithm with polynomials up to 12th order, depending on the desired precision.

By employing the A-M algorithm, much larger time-steps than those required by the Newmark method could be used. However, a very restrictive tolerance was still required, as long as the phase of the oscillations — and therefore the "choice" of the final potential well — showed to be strongly dependent on it.

4.2 Parameters Choices

As stated above, the system parameters used in this work are $L = 1.0$, $\ell_0 = \sqrt{2}$, $k = 4\pi^2$, and $m = 1$. We can also define from these parameters two characteristic times of the system :

$$\tau_1 = 4\pi^2 m/k$$
$$\tau_2 = 2m/c \quad ,$$

where c is the linear damping factor.

In a linear oscillator, τ_1 would be the simply the system period and τ_2 the energy decay time constant. This is also true for our system, at large oscillations regime. In a nonlinear regime, the constant τ_2 still approaches a characteristic energy loss time. For the non dimensional ratio τ_2/τ_1 we used the values 10, 20, 40, and 80.

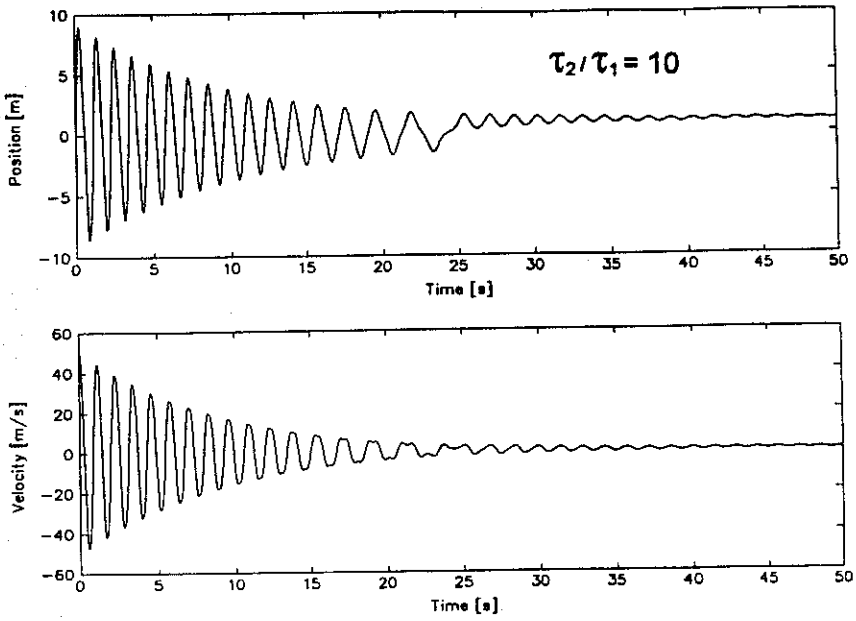

Fig. 6. Time history of damped oscillations, $\tau_2/\tau_1 = 10$: a) position; b) velocity history

The A-M algorithm was used to simulate the system transients. In order to keep comparable the results for different damping factors, we performed all the simulations with the same initial velocity $v_0 = 50{,}0$. This value corresponds to large oscillations, with a near linear force regime. The length of the simulations is five times the time constant τ_2, so that the system undergoes roughly through the same energy contents in all simulations.

The simulation time step is $Dt = 0.001$ s, so that the longest simulation involves 400,000 time steps. The record actually stores one out of 50 time steps, so that the final time steps have $Dt = 0.5$ s.

4.3 Comments on the Solutions

The results of the simulations of the ST system are shown in figures 6, 7, 8, and 9 with position (a) and velocity (b) as a function of the dimensionless parameter τ_2/τ_1. In all simulations it is possible to identify two distinct regions, both with a monotonous amplitude decrease, separated by a sudden discontinuity. In this "step", the amplitude suffers an abrupt reduction, in the neighbourhood of the time t/τ_1 0.5. This change happens when the system energy reaches the same value as the potential "hill" in the middle of the potential curve. Below this limit the mass can no longer travel between the two potential wells and is confined to one of them. The return points change, and so does the amplitude.

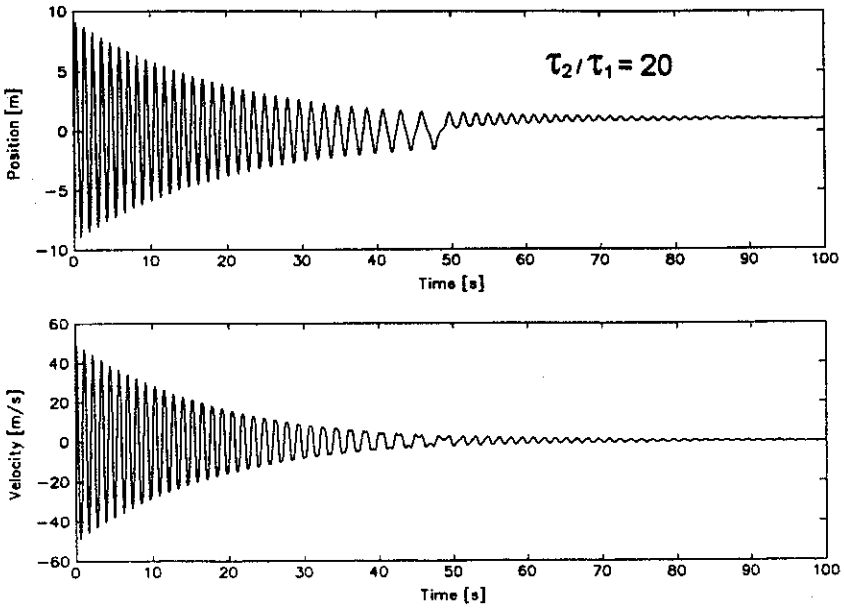

Fig. 7. Time history of damped oscillations, $\tau_2/\tau_1 = 20$: a) position; b) velocity history

The amplitude "step" is less dramatic than it could appear in a first sight. Although there is a sudden change in amplitude in the *position* history, there is a continuity in the energy content of the system. This can be seen by inspection in the *velocity* history plots of, whose local maxima and minima correspond to the total energy. The velocity envelope does not show discontinuities.

This abrupt change on movement regime is essentially different from the jump phenomena that occurs on *forced* nonlinear oscillators (Stoker, 1950), (Abramson, 1961), (Nayfeh, 1979). In the case of a forced "hardening" or "softening" systems, jumps are expected to occur. They arise when the oscillating force reaches an unstable solution range of parameters. In the snap through system, the *"pseudo-jump"* above described occurs in the absence of an external force.

We show on figure 10 the system trajectory in the phase space, for $\tau_2/\tau_1 = 40$. The first points were skipped and the trajectory starts near the "pseudo-jump". The system first transits across both potential wells. After the "pseudo-jump", the trajectory moves across a single potential well. There is a clear change in the movement regime. The energy loss per cycle becomes smaller, since the area enclosed between two successive cycles shrinks. The system moves toward one of the point attractor and orbits approach a circular form, since the oscillations become linear.

The simulation of the equivalent unforced Duffing equation yields similar results,

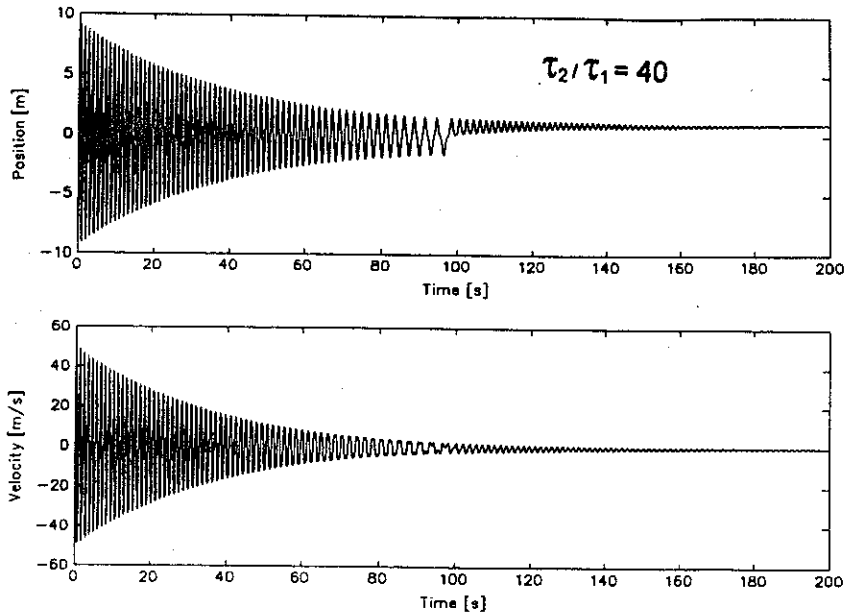

Fig. 8. Time history of damped oscillations, $\tau_2/\tau_1 = 40$: a) position; b) velocity history

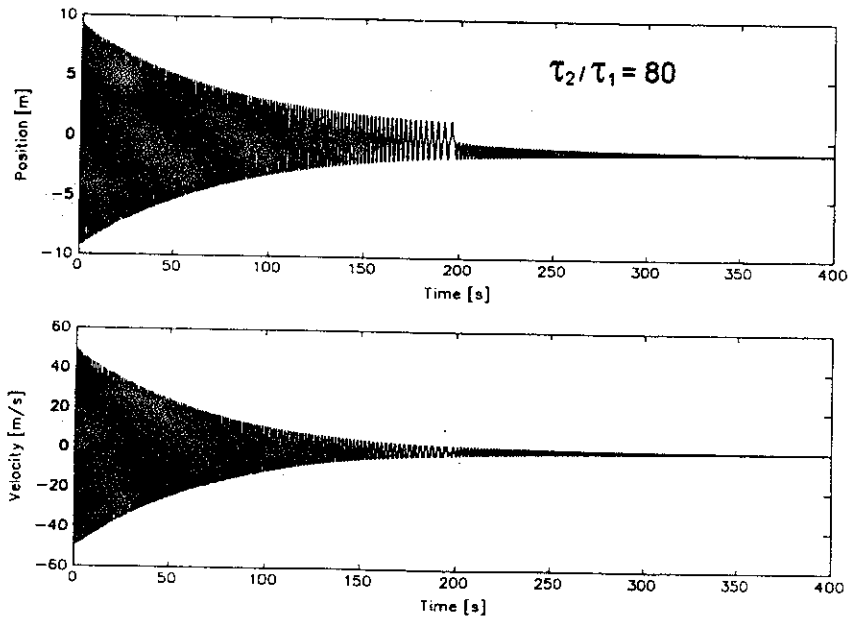

Fig. 9. Time history of damped oscillations, $\tau_2/\tau_1 = 80$: a) position; b) velocity history

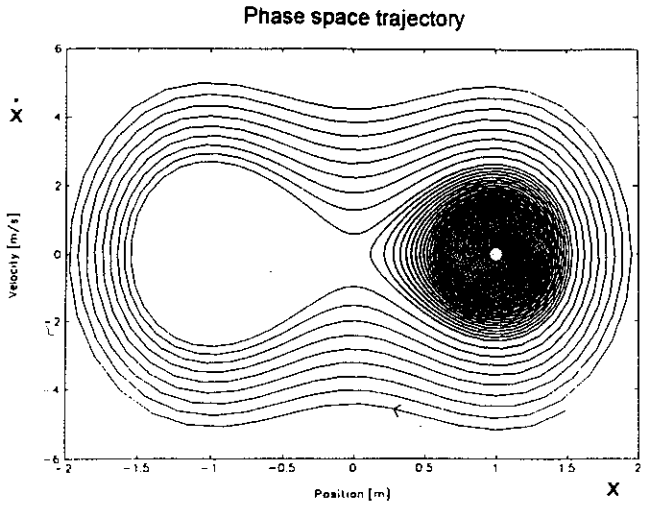

Fig. 10. Phase-space trajectory of the *snap-through* system $\tau_2/\tau_1 = 40$. The system exhibits two different regimes (see text).

so that the visual aspect of both is essentially the same. For this reason, the time histories of the Duffing equation are not shown. However their spectrograms reveal many differences that will be discussed below.

5 Analysis of Gabor Spectrograms

The Gabor Transform has a single adjustable parameter, the frequency spacing between the "filters" or "voices". We first performed the transformation with spacing of 0.05, 0.1, 0.2 and 0.4 Hz and then selected the $Df = 0.1$ Hz, one tenth of the natural frequency in the large amplitude limit, which yielded the best global visibility for the involved phenomena. The Gabor spectrograms are calculated directly from equations (2, 3, 4). The wave packets were first evaluated for every Gabor grid frequency and then pointwise multiplied by the *velocity* time history points.

The calculations are performed over a *finite* number of points. However, the calculated wave packets, with a length of 800 points, had the absolute value in the edge that was about 10^{-10} of the top value. The contribution of the points outside this range is smaller than the numerical uncertainty of the simulation points, so that the effects of the use of a finite number of points are negligible.

An oversampling factor of 2× for the frequency scale and 4× for time scale was used to smooth the spectrogram and adjust its final aspect ratio. The output of the analysis is then a 200×320 complex matrix. In this work, only the amplitudes are analysed. In order to improve the visibility of higher order harmonics, we "compressed" the amplitude scale by taking its *logarithm*.

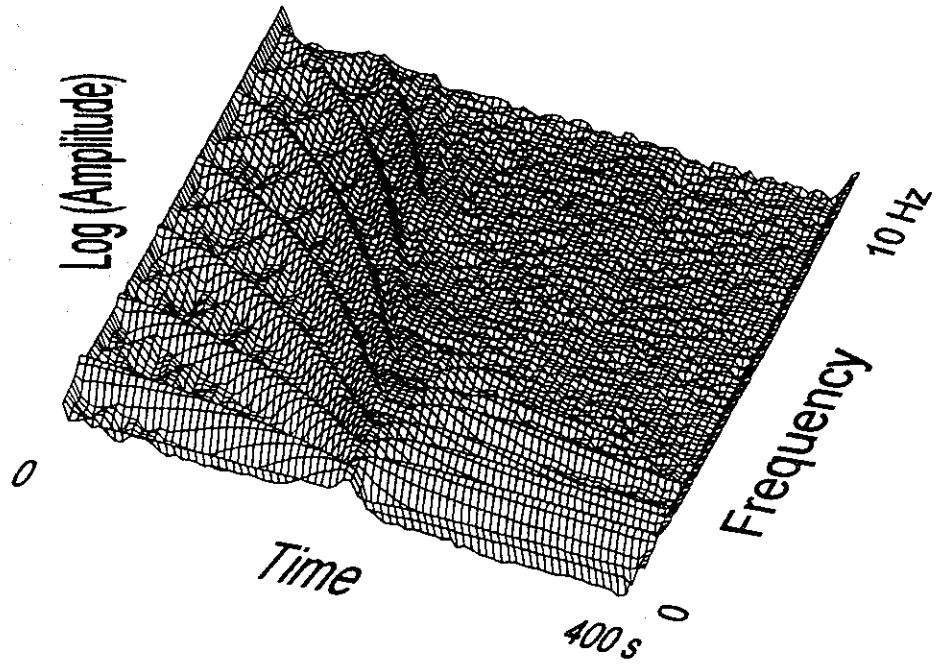

Fig. 11. Gabor spectrogram of the *snap-through* system for $\tau_1 = 40\,\mathrm{s}$. The "pseudo jump" is around the middle of the time domain. On the left side, a bundle of ridges describe the system dynamics when it oscillates across two potential wells. On the right side of the picture, a second ridge series is also visible.

We show in figure 11 a mesh graphic of the resulting GS. Each knot corresponds to a point in the Gabor grid, and the height is proportional to the logarithm of the amplitude at this point.

The mesh is bounded at the left and right edges by a tilted "wall". This effect is a result of a discontinuity that naturally exists in the beginning and the end of the finite simulation. The abrupt step from a finite value to zero has spectral components in all frequencies, which appears as a wall along the frequencies' axis. Such effect can be avoided by enlarging the simulation slightly beyond the region of interest, so that the edge walls are excluded. The region on a flat plain with slight irregularities, on the right top of the spectrogram, corresponds to a *digital noise* originated both from the integration of the DE and the calculation of the wave packets.

5.1 Aliasing Noise

Another sort of noise can also arise in digital spectral analysis. We can note that there are two bundles of "ridges" that cross each other in a *wafer* like structure on

the left half of the spectrogram. Only the high amplitude ridges truly correspond to physical effects, which we shall discuss below. The secondary smaller amplitude ridges are a *numerical* effect named *aliasing noise*.

The origin of the aliasing noise is the appearance of spurious frequencies when a fast oscillating function is sampled at a too low rate. It is analog to spurious rotating frequencies that can appear when a stroboscopic light illuminates a rotating wheel at a too low rate.

The aliasing noise is a well-studied effect of sampling rate, in the context of digital signal processing (Oppenheim, 1989); (Embree, 1991). The most economic sample rate that still contains all the information on a signal is, according to *Nyquist theorem*, the *double* of the higher frequency component. While in a true sampled signal it is possible to limit the incoming signal frequency band by a suitable *analog* filter, in the case of a simulation the high frequencies are inherently present on numerical integrations. If the simulation truly reflects the system behavior, it is not possible to eliminate the high frequencies present in the time history.

On the other hand, to increase the "sample rate" means also to increase in the number of time steps. This increases, however, the simulation and spectrogram computational overheads. Since the number of harmonics in a nonlinear oscillator is, in principle, infinite, the best we can is to decrease the aliasing noise amplitude. Although the intensity is supposed to decrease with the frequency, a necessary condition for solution convergence and finite energy, there is no sharp cut-off.

The signature of the aliasing noise is that the harmonics with a higher frequency than Nyquist frequency are mirrored into the lower frequency region. In our spectrogram, we can clearly see that the continuations of the high amplitude ridges to upper frequencies has been "folded" into the spectrogram range.

5.2 Color Spectrograms

The mesh plot has some inherent interpretation problems. The simulated 3-dimensional perspective can cause a peak or ridge to hide another. In the figure 11 spectrogram there is a second ensemble of ridges at the right side. Since the ridges overlap each other, it is difficult to examine them independently. An alternative method to translate the GS into a graphic is to use a flat colour map. Colours are then used to indicate different "heights" much as in a geographic elevation chart.

The colour scale we use here assigns the colours of the visible spectrum to the levels of amplitude logarithm. The higher amplitudes correspond to a saturated red, while the orange, yellow, green, blue and violet indicate successive decreasing amplitudes, with a total of 256 color hues.

5.3 Snap-Through System

The GS for $\tau_1 = 40$ is shown in figure 12a . The spectrum exhibits two bundles of red and orange tracks emerging from the middle of the time domain, around $t = 200\,\mathrm{s}$. Each track represents a sinusoidal function with a slowly varying frequency.

Colour changes in a track indicate a time-changing amplitude. We can conceive each track as a ridge in the time-frequency domain.

The left track bundle corresponds to the first stage of the time history, with large amplitude oscillations, where the mass crosses both potential wells. The lower frequency track or ridge corresponds to the time varying fundamental oscillation frequency along this stage. This track has a downward curvature and tends asymptotically to a frequency of about 1 Hz as time approaches zero, a consequence of the system geometry. As pointed out above, this system approaches a linear behaviour also for large amplitudes, so that the frequency approximates 1 Hz.

The large amplitude oscillations of the beginning of the time history, through locally periodic, are not exactly sinusoidal. Although the period approaches that of the linear oscillator, the nonlinear character of the restoring force near $x = 0$ distorts the oscillations. As a consequence, there should exist harmonics of this fundamental frequency. At the left edge, the track bundle indeed assumes asymptotically the form of a series of nearly horizontal lines. This is the GS counterpart of a harmonic series.

We can also note that this local frequency series has only *odd* multiples of the "fundamental" frequency. Since at the first stage of the simulation the mass transits across a symmetrical potential well, we expect each velocity cycle to be almost symmetric either. Since the Fourier transform of a symmetric function with period τ

$$s(t) = -s(t + \tau/2)$$

has only *odd harmonics*, a similar pattern appears locally in G S. This reflects the potential symmetry along the first stage.

Along the time-history, the fundamental frequency track migrates towards lower frequencies, while decreasing in amplitude. The whole left side track bundle follows this behaviour. Since the "fundamental frequency" is decreasing in frequency, the spacing between harmonics also shrinks. The whole structure eventually collapses around the time $t = 200\,\mathrm{s}$, where the system switches to a different regime with movements around a single potential well.

The right tracks bundle corresponds to single well oscillations. The fundamental track rises in frequency and tends to the frequency of small oscillations around the equilibrium point. This stage also shows a track series with frequencies that are *odd and even* integral multiples of the fundamental. The restoring force of a single potential well is no longer symmetric, so that the complete harmonic series appear. Motion symmetries are again reflected on GS.

As we approach the right edge of the spectrogram, the harmonic tracks vanish. Their amplitude decrease is expressed by a slow change in colour, drifting from red to yellow to blue, the latter being the numerical noise level. The vanishing harmonics indicate that the system approaches linearity and the motion tends to be purely sinusoidal as oscillations become small.

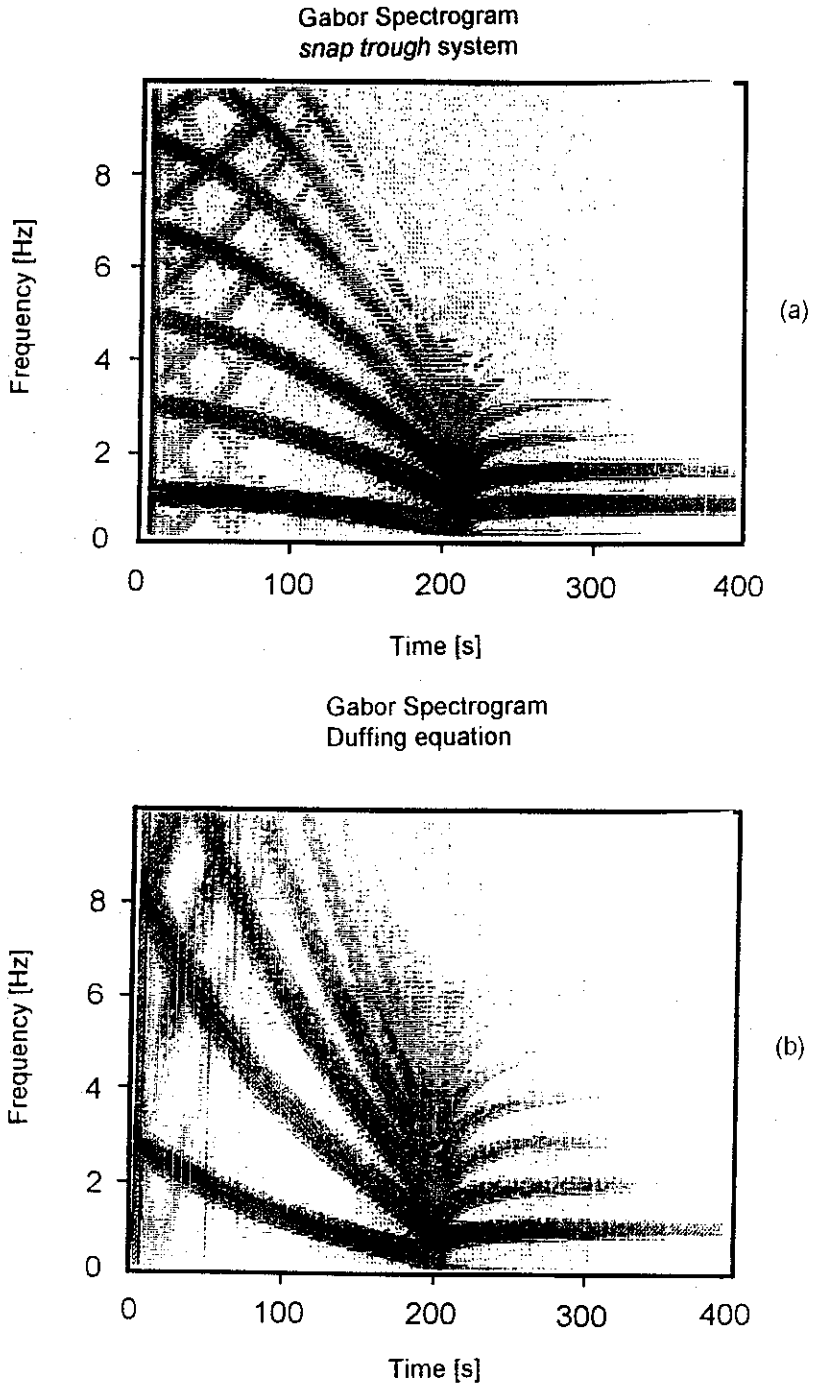

Fig. 12. Gabor spectrograms in color representation: a) *snap-through* system for $\tau_1 = 40\,\mathrm{s}$; b) unforced Duffing equation

5.4 Homogeneous (Unforced) Duffing Equation

This spectrogram (figure 12b) shows many qualitative features similar to the snap-through system. In particular the second phase of the time-history, on the right side of the spectrogram is virtually identical, since the Duffing equation was constructed as an expansion of the ST restoring force at the point $x = 0$. Some extra harmonics are visible at the second stage, a feature that can be attributed to different numerical noise levels.

The left track bundle shows some differences from the ST spectrogram. Since in the Duffing equation the cubic term can lead to arbitrarily high frequencies, the path of the fundamental track does not approximate any constant limit. The frequency grows continuously as we reach the larger amplitude region at the beginning of the time history. Since the symmetry of the potential well is similar to that of the ST system, we also have a track series with odd multiples of the fundamental frequency track.

6 Discussion and Conclusions

We employed Gabor spectrograms to analyze numerical simulations of a nonlinear system. They revealed a complex structure that contained essential features of the system dynamics. Moreover, patterns already familiar to FT users reappear in a generalized form, so that the results are easily readable. On the other hand, GS does not add new information about linear systems, where natural frequency does not change in time. It becomes helpful only on systems with frequency drifts.

The method proved to bring more enlightening results on cases where the energy loss per cycle is small compared to total energy, so that the system is nearly piecewise periodic. However, on a strongly damped system, the number of cycles is small and the very idea of local frequency becomes senseless. In this case GS, while still a complete expansion, does not bring new insight about system dynamics.

We expect that Gabor spectrograms of systems with chaotic behavior to show essentially the same results of the Fourier transform, in the stationary regime. No information about attractor dimensions can be directly extracted from GS. However, the wavelet transform, close related to GS, was already used to analyze fractals (Holschneider, 1988); (Arneodo*et al.*, 1988); (Ghez, 1991), and it is expected to reveal information about the attractor on chaotic systems. Nevertheless, the wavelet transform, due to its logarithmic character, eclipses some important signatures of non chaotic systems such as local periodicity. In non chaotic systems, the GS probably brings results of easier interpretation.

Although we analyzed here a particular system and parameters set, the same general procedure can also be adopted on a wide range of nonlinear systems. It is also a potentially good method to analyze other nonlinear phenomena such as forced oscillations, jumps and synchronization effects. GS can also be employed on a variety of experimental oscillation problems. Numerical implementation makes GS accessible to the analysis of virtually any physical variable that can be digitized.

Analog spectrogram methods have long been used to analyze the quite nonlinear musical instruments, as well as human voice and nature life sounds. Those old spectrograms used to have a rather narrow frequency range and were limited by the mathematical behaviour of real word components such as capacitors and coils. With the help of fast digital signal processing, spectrograms become also available to the analysis of numerical simulations. Furthermore, the use of Gaussian wave packets as a privileged expansion base, makes Gabor spectrogram an optimized tool in the analysis of nonlinear oscillations.

7 Acknowledgements

The authors acknowledge Dr. Nelson F. Ferrari for his helpful comments and stimulating discussions, and Dr. Aluisio F. Neves for the constant support in digital signal processing and other computational techniques.

References

Abramson, H.N.: 1961, 'Nonlinear Vibration', in *Shock and Vibration Handbook*, C.M. Harris and C.E. Crede eds., McGraw Hill Book Co., New York

Arneodo, A., Grasseau, G. and Holschneider, M.: 1988, 'Wavelet Transform of Multifractals', *Phys. Rev. Lett.* **Vol. 61 no. 20**, p. 2281

Banquet, J.P.: 1973, 'Spectral Analysis of the EEG in Meditation', *Eletroencephalography and Clinical Neurophysiology* **Vol. 35**, pp. 143–151

Bargmann, V. *et al.*: 1971, 'On the Completeness of the Coherent States', *Reports on Mathemetical Physics* **Vol. 2**, pp. 221–228

Bastiaans, M.J.: 1980, 'Gabor's Expansion of a Signal into Gaussian Elementary Signals', *Proceedings of the I.E.E.E.* **Vol. 68**, pp. 538-539

Bathe, K.J. and Wilson, E.L.: 1989, 'Numerical Methods in Finite Element Analysis',Prentice Hall, Inc., New Jersey

Belogorstev, A.B.: 1992, 'Bifurcations of Tori and Chaos in the Quasiperiodically Forced Duffing Oscillator', *Nonlinearity* **Vol. 5**, p. 889

Combes, J.M., Grossmann, A. and Ph. Tchamitchian (Editors): 1987, 'Wavelets, Time-Frequency Methods and Phase Space', Proceedings of the International Conference, Marseille, France

Courant, R. and Hilbert, D.: 1953, 'Methods of Mathematical Physics', Interscience, New York

Curtis, F.G. and Wheatley, P.O.: 1989, 'Applied Numerical Analysis', Adison Wesley Pub. Co.

Daubechies, I.: 1990, 'The Wavelet Transform, Time-Frequency Localization and Signal Analysis', *IEEE Transactions on Information Theory* **Vol. IT-36**, pp. 961–1005

Daubechies, I, Mallat, S. and Willsky, A.S.: 1992, 'Introduction to the Special Issue [on Wavelet Transforms and Multirresolution Signal Analysis]', *IEEE Transactions on Information Theory* **Vol. 38 no. 2**, p. 529.

Embree, P. M. and Kimble, B.: 1991, 'C Language Algorithms for Digital Processing', Prentice Hall, Englewood Cliffs (N. Jersey)

Franco, H., Ribeiro, C., Caldas I.L., da Silva, R.P. and Galvão, R.M.O.: 1992, 'Time-Resolved Analysis of Mirnov Oscillations, *Review of Scientific Instruments* **Vol. 63**, pp. 3710–3715

Gabor, D.: 1946, 'Theory of Communication', *Journal of the Institution of Eletrical Engeneers* part III, **Vol. 93**, pp. 429–441

Ghez, J-M. and Vaienti, S.: 1991, 'Integrated Wavelets on Fractal Sets: I. The correlation dimension', *Nonlinearity* **5**, p. 777

Ghez, J-M and Vaienti, S.: 1991, 'Integrated Wavelets on Fractal Sets: II. The Generalized Dimensions", *Nonlinearity* **5**, p. 791

Grossman, A. and Morlet: 1984, 'Decomposition of Hardy Functions into Square Integrable Wavelets of Constant Shape', *SIAM Journal of Mathematical Analysis* **Vol. 15 no. 4**, pp. 723–736

Helstrom, Carl W.: 1966, 'An Expansion of a Signal in Gaussian Elementary Signals', *IEEE Transactions on Information Theory* **Vol. IT-12**, p. 81–82

Holmes, P.: 'A Nonlinear Oscillator With a Strange Attractor' *Philosophical Transactions of the Royal Society* **Vol. 292A**, p. 1394

Holschneider, M.: 'On The Wavelet Transform of Fractal Objects', *Journal of Statistical Physics* **Vol. 50**, p. 963

Huang, N.C. and Nachbar, W.: *Trans. A.S.M.E. Jl appl. Mech.* **Vol. 44**, pp. 147–155

Huseyin, K.: 1975, 'Nonlinear Theory of Elastic Stability', Noordhoff Int. Pub., Leyden

Kahaner, D., Moler, C. and Nash, S.: 1989, 'Numerical Methods and Software', Prentice Hall

Karaesmen, E.: 1988, 'Chaotic Dynamic Analysis of Viscoelastic Shallow Spherical Shells', *Computers and Structures* **Vol. 44 no. 4**, p. 851–857

Kroland-Martinet, R.: 1988, 'The Wavelet Analysis, Synthesis, and Processing of Speech and Music Sounds', *Computer Music Journal* **Vol. 12 no. 4**, p. 11–20

Lichtenberg, A.J. and Lieberman, M.A.: 'Regular and Stochastic Motion', Springer-Verlag, New York

Meyer, Y.: 1989, 'Ondelettes et Operateurs', Herman Editeurs des Sciences et des Arts, Paris

Morlet, J. *et al.*: 1982A, 'Wave Propagation and Sampling Theory - Part II: Sampling Theory and Complex Waves', *Geophysics* **Vol. 47 no. 2**, pp. 222–236

Morlet, J. *et al.*: 1982B, 'Wave Propagation and Sampling Theory - Part II: Complex Signal and Scattering in Multilayered Media', *Geophysics* **Vol. 47 no. 2**, pp. 203–221

Nayfeh A.H.: 1979, 'Nonlinear Oscillations', Willey Interscience, New York

Oppenheim, A.V. and Schafer, R.W.: 1989, 'Discrete Time Signal Processing', Prentice Hall, Inc., N.J.

Perelomov, A.M.: 1971, 'On the Completeness of a System of Coherent States', *Theor. Math. Phys.* **Vol. 6**, pp. 156-164.

Quian, S. and Chen, K.: 1992 A, *Signal Processing* **Vol. 27**, p. 125

Quian, S. and Chen, K.: 1992 B, *Signal Processing* **Vol. 27**, p. 177

Schiff, L.I.: 1955, 'Quantum Mechanics' (2nd ed.), McGraw Hill Book Co., New York

Simitses, G.J.: 1990, 'Dynamic Stability of Suddenly Loaded Structures', Springer Verlag, New York

Stoker, J.J.: 1950, 'Nonlinear Vibrations in Mechanical and Electrical Systems', Interscience Publishers, New York

Thompson, J.M.T. and Hunt, G.W.: 1973, 'A General Theory of Elastic Stability', John Willey & Sons, London

Thompson, J.M.T. and Hunt, G.W.: 1984, 'Elastic Instability Phenomena', John Willey & Sons, London

Thompson, J.M.T. and Steward, H.B.: 1987, 'Nonlinear Dynamics and Chaos', John Willey & Sons, Chichester

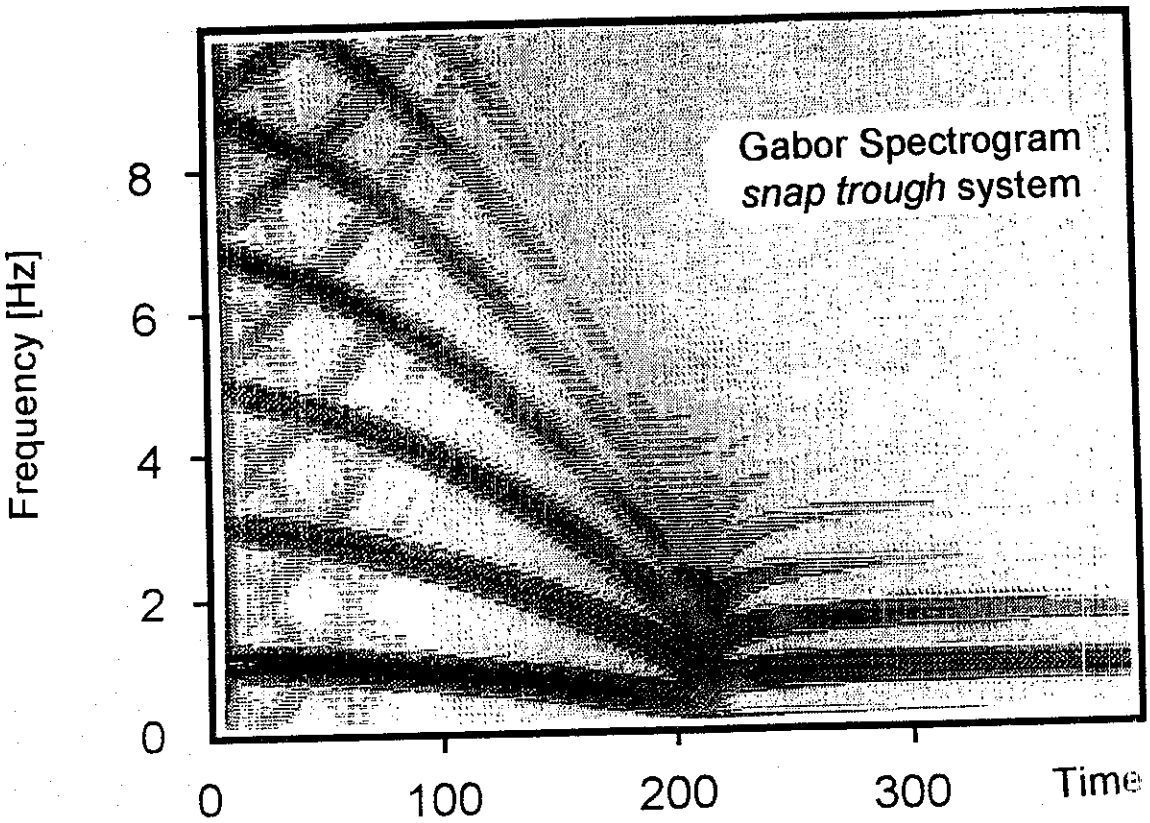

(a

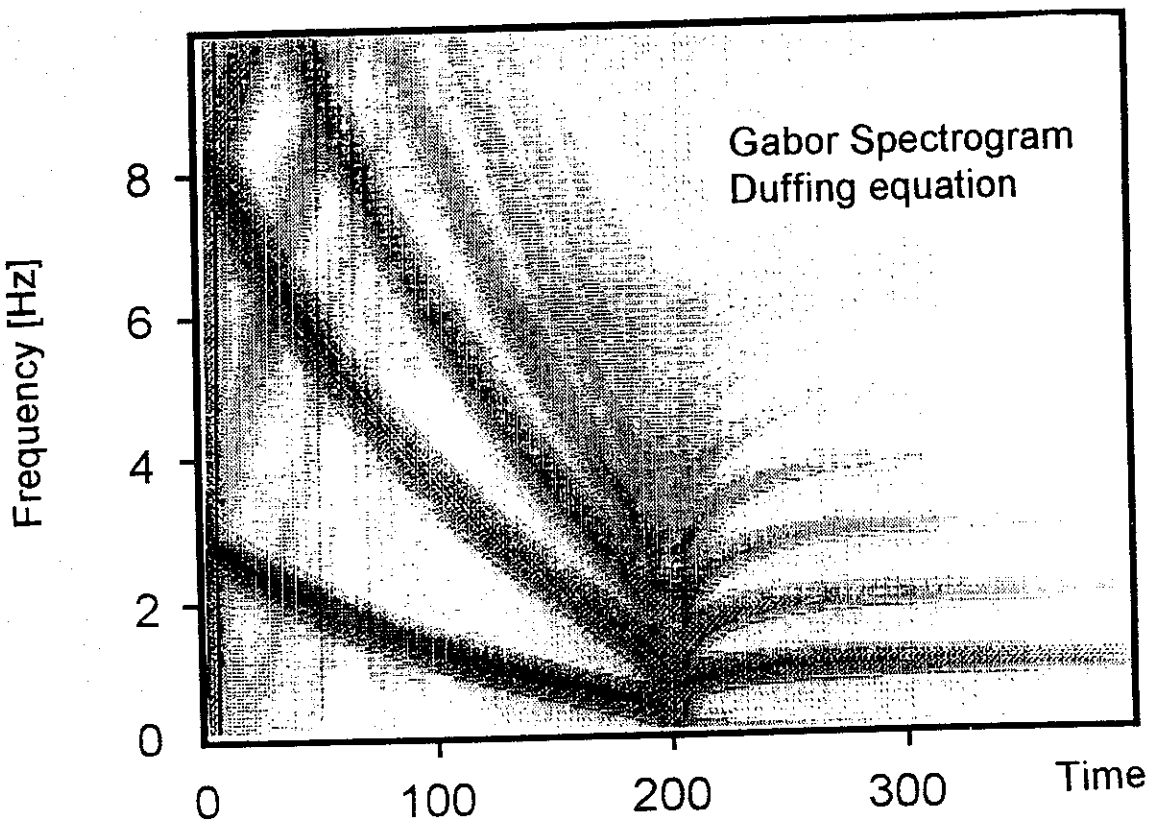

Figures 12 a and b are color pictures. We show above a gray level version, made on a dot matrix printer and more appropriated to black & white *preprint* copies.